

# Canonical symplectic particle-in-cell method for long-term large-scale simulations of the Vlasov-Maxwell system

Hong Qin,<sup>1,2</sup> Jian Liu,<sup>1,3</sup> Jianyuan Xiao,<sup>1,3</sup> Ruili Zhang,<sup>1,3</sup> Yang He,<sup>1,3</sup> Yulei Wang,<sup>1,3</sup> Yajuan Sun,<sup>4</sup> Joshua W. Burby,<sup>2</sup> Leland Ellison,<sup>2</sup> and Yao Zhou<sup>2</sup>

<sup>1</sup>*School of Nuclear Science and Technology and Department of Modern Physics, University of Science and Technology of China, Hefei, Anhui 230026, China*

<sup>2</sup>*Plasma Physics Laboratory, Princeton University, Princeton, NJ 08543*

<sup>3</sup>*Key Laboratory of Geospace Environment, CAS, Hefei, Anhui 230026, China*

<sup>4</sup>*LSEC, Academy of Mathematics and Systems Science, Chinese Academy of Sciences, P.O. Box 2719, Beijing 100190, China*

## Abstract

Particle-in-Cell (PIC) simulation is the most important numerical tool in plasma physics. However, its long-term accuracy has not been established. To overcome this difficulty, we developed a canonical symplectic PIC method for the Vlasov-Maxwell system by discretizing its canonical Poisson bracket. A fast local algorithm to solve the symplectic implicit time advance is discovered without root searching or global matrix inversion, enabling applications of the proposed method to very large-scale plasma simulations with many, e.g.,  $10^9$ , degrees of freedom. The long-term accuracy and fidelity of the algorithm enables us to numerically confirm Mouhot and Villani's theory and conjecture on nonlinear Landau damping over several orders of magnitude using the PIC method, and to calculate the nonlinear evolution of the reflectivity during the mode conversion process from extraordinary waves to Bernstein waves.

PACS numbers: 52.65.Rr, 52.25.Dg

In modern plasma physics, numerically solving the Vlasov-Maxwell (VM) equations using the Particle-In-Cell (PIC) method has become the most important tool [1, 2] for theoretical studies in the last half century. Many innovative algorithms, such as the Boris scheme for advancing particles [3, 4] and Villasenor-Buneman’s charge-conserving deposition scheme [5], have been developed and successfully applied. Recently, new geometric numerical methodology has been adopted for PIC simulations. This exciting trend begins with the discovery of symplectic algorithms for Hamiltonian equations that govern charged particle dynamics [6–16]. The Boris algorithm was discovered to be volume-preserving [17, 18] and high-order volume-preserving methods have been found [19]. In addition, the Vlasov-Maxwell system [20–24] and the Vlasov-Poisson system [25] have been discretized from a variational symplectic perspective that preserves symplectic structures and exhibits excellent long-term accuracy and fidelity.

In this letter, we develop a new canonical symplectic PIC method for solving the VM equations by discretizing its canonical Poisson bracket [26]. The distribution function  $f$  is first discretized in phase space through the Klimontovich representation by a finite number of Lagrangian sampling points  $(\mathbf{X}_i, \mathbf{P}_i)$  ( $i = 1, \dots, N$ ), where  $\mathbf{X}_i$  and  $\mathbf{P}_i$  are the position and canonical momentum of the  $i$ -th particle, and  $N$  is the total number of sampling points. The electromagnetic field is discretized point-wise on a given spatial grid, and the Hamiltonian functional is expressed as a function of the sampling points and the discretized electromagnetic field. This procedure generates a finite-dimensional Hamiltonian system with a canonical symplectic structure. The number of degrees of freedom for the discrete system is  $D = 3N + 3M$ , where  $M$  denotes the total number of the discrete grid-points.

In general, for a Hamiltonian function whose momentum dependence and position dependence are not separable, it is not possible to make symplectic integration algorithms explicit [9, 14]. For the discrete Hamiltonian system developed here for the VM equations, the dimension of system is usually very large, and root searching algorithms required by implicit methods are too time-consuming to be practical. However, we discovered that if the symplectic Euler algorithm [9] is applied to the discrete VM Hamiltonian system at hand, the implicit time advance can be carried out as inexpensively as an explicit method by just inverting a  $3 \times 3$  matrix for every particle separately. The resulting canonical symplectic PIC method for the VM system inherits all the good numerical features of canonical symplectic algorithms, such as the long-term bound on energy-momentum error. Being symplectic

means that the numerical solution satisfies  $D(2D - 1)$  constraints as the exact solution does. Since  $D$  is a large number, the symplectic condition is much stronger than a few constraints on global energy and momentum. The symplectic condition is almost as strong as imposing local conservation everywhere in phase space.

Two examples of application are given. In the first example, we simulate the dynamics of nonlinear Landau damping. It also serves as a test of the algorithm. The discrete VM Hamiltonian system for this study has more than  $2.69 \times 10^8$  degrees of freedom. The damping rate from the numerical results agrees exactly with the theoretical result. Furthermore, long-term simulations reveal that the phase mixing dynamics in velocity space is the physical mechanism of the nonlinear Landau damping, as recently proved by Mouhot and Villani [27, 28] for the Vlasov-Poisson system and conjectured by Villani [29] for the Vlasov-Maxwell system. In the second application, we study the nonlinear mode conversion process from extraordinary modes to Bernstein modes (X-B mode conversion) in an inhomogeneous hot plasma. Simulations show that nonlinear mode excitations and self-interaction of the Bernstein waves significantly modify the reflectivity and conversion rate. It is the long-term accuracy and fidelity of the canonical symplectic PIC algorithm that enables us to numerically confirm Mouhot and Villani's theory and conjecture over several orders of magnitude using the PIC method, and to calculate the nonlinear evolution of the reflectivity during the X-B mode conversion.

We start from the canonical Poisson bracket and Hamiltonian for the Vlasov-Maxwell equations [26],

$$\{F, G\} \equiv \int f \left\{ \frac{\delta F}{\delta f}, \frac{\delta G}{\delta f} \right\}_{\mathbf{x}\mathbf{p}} d\mathbf{x}d\mathbf{p} + \int \left( \frac{\delta F}{\delta \mathbf{A}} \frac{\delta G}{\delta \mathbf{Y}} - \frac{\delta G}{\delta \mathbf{A}} \frac{\delta F}{\delta \mathbf{Y}} \right) d\mathbf{x}. \quad (1)$$

$$H(f, \mathbf{A}, \mathbf{Y}) = \frac{1}{2} \int (\mathbf{p} - \mathbf{A})^2 f d\mathbf{x}d\mathbf{p} + \frac{1}{2} \int [\mathbf{Y}^2 + (\nabla \times \mathbf{A})^2] d\mathbf{x}. \quad (2)$$

Here,  $F$ ,  $G$ , and the Hamiltonian  $H$  are functionals of the distribution function  $f$ , vector potential  $\mathbf{A}$ , and  $\mathbf{Y} \equiv \partial \mathbf{A} / \partial t$ . The bracket  $\{h, g\}_{\mathbf{x}\mathbf{p}}$  inside the first term on the right hand side of Eq. (1) is the canonical Poisson bracket for functions  $h$  and  $g$  of canonical phase space  $(\mathbf{x}, \mathbf{p})$ . The temporal gauge, i.e.,  $\phi = 0$ , has been explicitly chosen for this Poisson bracket to be valid. The Poisson bracket defined in Eq. (1) can be formally derived from the point of view of co-adjoint orbit theory [26], and can be used to derive the non-canonical Morrison-Marsden-Weinstein bracket in the  $(f, \mathbf{E}, \mathbf{B})$  and  $(\mathbf{x}, \mathbf{v})$  coordinates [26, 30, 31]. First, we

discretize the distribution function using the Klimontovich representation

$$f(\mathbf{x}, \mathbf{p}, t) = \sum_{i=1}^N \delta(\mathbf{x} - \mathbf{X}_i) \delta(\mathbf{p} - \mathbf{P}_i), \quad (3)$$

where  $(\mathbf{X}_i, \mathbf{P}_i)$  ( $i = 1, \dots, N$ ) are particles' coordinates in phase space. Under this discretization, it can be shown that

$$\frac{\delta F}{\delta \mathbf{X}_i} = \int \delta(\mathbf{x} - \mathbf{X}_i) \delta(\mathbf{p} - \mathbf{P}_i) \frac{\partial}{\partial \mathbf{x}} \left( \frac{\delta F}{\delta f} \right) d\mathbf{x} d\mathbf{p}, \quad (4)$$

$$\frac{\delta F}{\delta \mathbf{P}_i} = \int \delta(\mathbf{x} - \mathbf{X}_i) \delta(\mathbf{p} - \mathbf{P}_i) \frac{\partial}{\partial \mathbf{p}} \left( \frac{\delta F}{\delta f} \right) d\mathbf{x} d\mathbf{p}, \quad (5)$$

from which we obtain

$$\frac{\delta F}{\delta \mathbf{X}_i} \frac{\delta G}{\delta \mathbf{P}_i} - \frac{\delta G}{\delta \mathbf{X}_i} \frac{\delta F}{\delta \mathbf{P}_i} = \int \delta(\mathbf{x} - \mathbf{X}_i) \delta(\mathbf{p} - \mathbf{P}_i) \left\{ \frac{\delta F}{\delta f}, \frac{\delta G}{\delta f} \right\}_{\mathbf{x}\mathbf{p}} d\mathbf{x} d\mathbf{p}. \quad (6)$$

It then follows that the first term on the right-hand side of Eq. (1) is

$$\int f \left\{ \frac{\delta F}{\delta f}, \frac{\delta G}{\delta f} \right\}_{\mathbf{x}\mathbf{p}} d\mathbf{x} d\mathbf{p} = \sum_{i=1}^N \left( \frac{\delta F}{\delta \mathbf{X}_i} \frac{\delta G}{\delta \mathbf{P}_i} - \frac{\delta G}{\delta \mathbf{X}_i} \frac{\delta F}{\delta \mathbf{P}_i} \right). \quad (7)$$

Similar derivation of the discretized bracket can be found in the context of Hamiltonian description of vortex fluid [32, 33].

To discretize the second term on the right-hand side of Eq. (1), we first discretize the fields  $\mathbf{A}(t)$  and  $\mathbf{Y}(t)$  on a Eulerian spatial grid as

$$\mathbf{A}(\mathbf{x}, t) = \sum_{J=1}^M \mathbf{A}_J(t) \Psi(\mathbf{x} - \mathbf{x}_J), \quad \mathbf{Y}(\mathbf{x}, t) = \sum_{J=1}^M \mathbf{Y}_J(t) \Psi(\mathbf{x} - \mathbf{x}_J), \quad (8)$$

where the discrete fields  $\mathbf{A}_J(t)$  and  $\mathbf{Y}_J(t)$  are the fields evaluated on the grid-point  $\mathbf{x}_J$ . The subscript  $J$  is the index of the grid-point, and  $M$  is the total number of the grid-points. Here,  $\Psi(\mathbf{x} - \mathbf{x}_J)$  is the step function,

$$\Psi(\mathbf{x} - \mathbf{x}_J) = \begin{cases} 1, & |x - x_J| < \frac{\Delta x}{2}, |y - y_J| < \frac{\Delta y}{2}, |z - z_J| < \frac{\Delta z}{2}, \\ 0, & \text{elsewhere.} \end{cases} \quad (9)$$

Under this discretization of  $\mathbf{A}(t)$  and  $\mathbf{Y}(t)$ , we have

$$\frac{\delta F}{\delta \mathbf{A}} = \sum_{J=1}^M \frac{\delta \mathbf{A}_J}{\delta \mathbf{A}} \frac{\partial F}{\partial \mathbf{A}_J} = \sum_{J=1}^M \frac{1}{\Delta V} \Psi(\mathbf{x} - \mathbf{x}_J) \frac{\partial F}{\partial \mathbf{A}_J}, \quad (10)$$

where  $\Delta V$  is the volume of each cell, which is taken to be a constant in the present study.

For the second equal sign in Eq. (10), use has been made of the fact that

$$\frac{\delta \mathbf{A}_J}{\delta \mathbf{A}} = \frac{1}{\Delta V} \Psi(\mathbf{x} - \mathbf{x}_J). \quad (11)$$

The discretization of the second term on the right-hand side of Eq. (1) is thus

$$\int \left( \frac{\delta F}{\delta \mathbf{A}} \frac{\delta G}{\delta \mathbf{Y}} - \frac{\delta G}{\delta \mathbf{A}} \frac{\delta F}{\delta \mathbf{Y}} \right) d\mathbf{x} = \sum_{J=1}^M \left( \frac{\partial F}{\partial \mathbf{A}_J} \frac{\partial G}{\partial \mathbf{Y}_J} - \frac{\partial G}{\partial \mathbf{A}_J} \frac{\partial F}{\partial \mathbf{Y}_J} \right) \frac{1}{\Delta V}. \quad (12)$$

Finally, the discrete Poisson bracket for the VM system is

$$\{F, G\} = \sum_{i=1}^N \left( \frac{\delta F}{\delta \mathbf{X}_i} \frac{\delta G}{\delta \mathbf{P}_i} - \frac{\delta G}{\delta \mathbf{X}_i} \frac{\delta F}{\delta \mathbf{P}_i} \right) + \sum_{J=1}^M \left( \frac{\partial F}{\partial \mathbf{A}_J} \frac{\partial G}{\partial \mathbf{Y}_J} - \frac{\partial G}{\partial \mathbf{A}_J} \frac{\partial F}{\partial \mathbf{Y}_J} \right) \frac{1}{\Delta V} \quad (13)$$

for functions  $F$  and  $G$  of the particles  $(\mathbf{X}_i, \mathbf{P}_i)$  and the discretized field  $(\mathbf{A}_J, \mathbf{Y}_J)$ .

Next, we need to express the Hamiltonian functional given by Eq. (2) in terms of  $(\mathbf{X}_i, \mathbf{P}_i)$  and  $(\mathbf{A}_J, \mathbf{Y}_J)$ . The particles' total kinetic energy is the sum of each particle's kinetic energy. The vector potential at a particle's position can be interpolated from  $\mathbf{A}_J(t)$  as

$$\mathbf{A}(\mathbf{X}_j, t) = \sum_{J=1}^M \mathbf{A}_J(t) W(\mathbf{X}_j - \mathbf{x}_J), \quad (14)$$

where  $W(\mathbf{X}_j - \mathbf{x}_J)$  is a chosen interpolation function. Note that  $W(\mathbf{X}_j - \mathbf{x}_J)$  is not necessarily the same as the step function  $\Psi(\mathbf{x} - \mathbf{x}_J)$  in Eq. (8). This is of course allowed as long as the consistency condition is satisfied, i.e., the continuous limit is recovered when the grid-size goes to zero. The Hamiltonian then becomes

$$\begin{aligned} \tilde{H}(\mathbf{X}_i, \mathbf{P}_i, \mathbf{A}_J, \mathbf{Y}_J) = & \frac{1}{2} \sum_{i=1}^N \left( \mathbf{P}_i^2 - 2\mathbf{P}_i \cdot \sum_{J=1}^M \mathbf{A}_J W(\mathbf{X}_i - \mathbf{x}_J) \right. \\ & \left. \sum_{J,L=1}^M \mathbf{A}_J \cdot \mathbf{A}_L W(\mathbf{X}_i - \mathbf{x}_J) W(\mathbf{X}_i - \mathbf{x}_L) \right) + \frac{1}{2} \sum_{J=1}^M [\mathbf{Y}_J^2 + (\nabla_d \times \mathbf{A})_J^2] \Delta V, \quad (15) \end{aligned}$$

where  $(\nabla_d \times \mathbf{A})_J$  is the discrete curl operator acting on the discrete vector potential evaluated at the  $J$ -th grid-point. Finally, the discrete Hamiltonian (15) and discrete Poisson structure (13) form a canonical symplectic discretization of the original continuous Vlasov-Maxwell system. The ordinary differential equations for the canonical system are

$$\dot{\mathbf{X}}_i = \left\{ \mathbf{X}_i, \tilde{H} \right\}_d = \mathbf{P}_i - \sum_{J=1}^M \mathbf{A}_J W(\mathbf{X}_i - \mathbf{x}_J), \quad (16)$$

$$\dot{\mathbf{A}}_J = \left\{ \mathbf{A}_J, \tilde{H} \right\}_d = \mathbf{Y}_J, \quad (17)$$

$$\begin{aligned} \dot{\mathbf{P}}_i = \left\{ \mathbf{P}_i, \tilde{H} \right\}_d = & \sum_{J=1}^M (\mathbf{P}_i \cdot \mathbf{A}_J) \nabla W(\mathbf{X}_i - \mathbf{x}_J) - \\ & \sum_{J,L=1}^M (\mathbf{A}_J \cdot \mathbf{A}_L) W(\mathbf{X}_i - \mathbf{x}_J) \nabla W(\mathbf{X}_i - \mathbf{x}_L), \end{aligned} \quad (18)$$

$$\begin{aligned} \dot{\mathbf{Y}}_J = \left\{ \mathbf{Y}_J, \tilde{H} \right\}_d = & \sum_{i=1}^N \mathbf{P}_i W(\mathbf{X}_i - \mathbf{x}_J) \frac{1}{\Delta V} - \\ & \sum_{i=1}^N \sum_{L=1}^M \mathbf{A}_L W(\mathbf{X}_i - \mathbf{x}_J) W(\mathbf{X}_i - \mathbf{x}_L) \frac{1}{\Delta V} - \left( \nabla_d^T \times \nabla_d \times \mathbf{A} \right)_J. \end{aligned} \quad (19)$$

This equation system consists of  $6(M+N)$  equations describing the dynamics of  $N$  particles and fields on  $M$  discrete grid-points. The last term in Eq. (19) is defined to be

$$\left( \nabla_d^T \times \nabla_d \times \mathbf{A} \right)_J \equiv \frac{1}{2} \frac{\partial}{\partial A_J} \left[ \sum_{L=1}^M (\nabla_d \times \mathbf{A})_L^2 \right]. \quad (20)$$

The notation of  $\nabla_d^T \times \nabla_d \times \mathbf{A}$  indicates that the right hand side of Eq. (20) can be viewed as the discretized  $\nabla \times \nabla \times \mathbf{A}$  for a well-chosen discrete curl operator  $\nabla_d$ . To wit, we note that the term  $\nabla \times \mathbf{A}$  in the Hamiltonian is discretized using the step function  $\Psi(\mathbf{x} - \mathbf{x}_J)$ ,

$$\nabla \times \mathbf{A} = \sum_{J=1}^M (\nabla_d \times \mathbf{A})_J \Psi(\mathbf{x} - \mathbf{x}_J). \quad (21)$$

As an example, we define the discrete curl operator  $(\nabla_d \times \mathbf{A})_J = (\nabla \times \mathbf{A})_{i,j,k}$  to be

$$\left( \nabla_d \times \mathbf{A} \right)_J \equiv \begin{pmatrix} \frac{A_{i,j,k}^3 - A_{i,j-1,k}^3}{\Delta y} - \frac{A_{i,j,k}^2 - A_{i,j,k-1}^2}{\Delta z} \\ \frac{A_{i,j,k}^1 - A_{i,j,k-1}^1}{\Delta z} - \frac{A_{i,j,k}^3 - A_{i-1,j,k}^3}{\Delta \mathbf{x}} \\ \frac{A_{i,j,k}^2 - A_{i-1,j,k}^2}{\Delta \mathbf{x}} - \frac{A_{i,j,k}^1 - A_{i,j-1,k}^1}{\Delta y} \end{pmatrix}, \quad (22)$$

which can be written as a linear operator on the space of  $3M$ -vectors as

$$\nabla_d \times \mathbf{A} = \begin{pmatrix} (\nabla_d \times \mathbf{A})_1 \\ \vdots \\ (\nabla_d \times \mathbf{A})_M \end{pmatrix} = \Gamma \begin{pmatrix} \mathbf{A}_1 \\ \vdots \\ \mathbf{A}_M \end{pmatrix}. \quad (23)$$

Here,  $\Gamma$  is a  $3M \times 3M$  sparse matrix specifying the discrete curl operator. The partial derivative with respect to  $\mathbf{A}_J$  can be expressed as

$$\frac{1}{2} \frac{\partial}{\partial \mathbf{A}_J} \left[ \sum_{L=1}^M (\nabla_d \times \mathbf{A})_L^2 \right] = \left[ \Gamma^T \Gamma \begin{pmatrix} \mathbf{A}_1 \\ \vdots \\ \mathbf{A}_M \end{pmatrix} \right]_J \equiv (\nabla_d^T \times \nabla_d \times \mathbf{A})_J, \quad (24)$$

where  $\Gamma^T$  is the transposition of  $\Gamma$ . Obviously, the notation in Eq. (20) or (24) is meaningful for any linear discrete curl operator  $\nabla_d$ .

It is clear from Eqs. (16)-(19) that the particles and fields interact through the interpolation function  $W(\mathbf{X}_i - \mathbf{x}_J)$ . The function  $W(\mathbf{X}_i - \mathbf{x}_J)/\Delta V$  distributes particles' charge over the grid-points as if they are "charged clouds" with finite-size [1].

Once the canonical symplectic structure is given, canonical symplectic algorithms can be readily constructed using well-developed methods [6–13]. For a reason soon to be clear, we adopt the semi-explicit symplectic Euler method for time advance. The symplectic Euler method for a generic canonical Hamiltonian system is

$$p^{n+1} = p^n - \Delta t \frac{\partial H}{\partial q}(p^{n+1}, q^n), \quad (25)$$

$$q^{n+1} = q^n + \Delta t \frac{\partial H}{\partial p}(p^{n+1}, q^n). \quad (26)$$

where  $\Delta t$  is the time-step, and the superscript  $n$  in  $p^n$  and  $q^n$  denotes that they are the value at the  $n$ -th time step. It is implicit for  $p$ , but explicit for  $q$ . Making use of this algorithm, the iteration rules for Eqs. (16) -(19) are

$$\frac{\mathbf{X}_i^{n+1} - \mathbf{X}_i^n}{\Delta t} = \mathbf{P}_i^{n+1} - \sum_{J=1}^M \mathbf{A}_J^n W(\mathbf{X}_i^n - \mathbf{x}_J), \quad (27)$$

$$\frac{\mathbf{A}_J^{n+1} - \mathbf{A}_J^n}{\Delta t} = \mathbf{Y}_J^{n+1}, \quad (28)$$

$$\begin{aligned} \frac{\mathbf{P}_i^{n+1} - \mathbf{P}_i^n}{\Delta t} &= \sum_{J=1}^M (\mathbf{P}_i^{n+1} \cdot \mathbf{A}_J^n) \nabla W(\mathbf{X}_i^n - \mathbf{x}_J) \\ &\quad - \sum_{J,L=1}^M (\mathbf{A}_J^n \cdot \mathbf{A}_L^n) W(\mathbf{X}_i^n - \mathbf{x}_J) \nabla W(\mathbf{X}_i^n - \mathbf{x}_L), \end{aligned} \quad (29)$$

$$\begin{aligned} \frac{\mathbf{Y}_J^{n+1} - \mathbf{Y}_J^n}{\Delta t} &= \sum_{i=1}^N \mathbf{P}_i^{n+1} W(\mathbf{X}_i^n - \mathbf{x}_J) \frac{1}{\Delta V} \\ &\quad - \sum_{i=1}^N \sum_{L=1}^M \mathbf{A}_L^n W(\mathbf{X}_i^n - \mathbf{x}_J) W(\mathbf{X}_i^n - \mathbf{x}_L) \frac{1}{\Delta V} - (\nabla_d^T \times \nabla_d \times \mathbf{A}^n)_J. \end{aligned} \quad (30)$$

These difference equations furnish a canonical symplectic PIC method for the Vlasov-Maxwell equations.

As discussed above, symplectic algorithms for a Hamiltonian system with non-separable momentum and position dependence are implicit in general. This is indeed the case for the difference equations (27)-(30), because the right-hand sides of Eqs. (27)-(30) depend on values of the  $(n + 1)$ -th time-step. However, they are semi-explicit, because Eqs. (27), (28), and (30) are explicit for  $\mathbf{X}_i^{n+1}$ ,  $\mathbf{A}_J^{n+1}$ , and  $\mathbf{Y}_J^{n+1}$ , respectively. Another good property of the system is that the only implicit equation (29) is linear in terms of  $\mathbf{P}_i^{n+1}$ , and it is only implicit for each particle, i.e., Eq. (29) does not couple  $\mathbf{P}_i^{n+1}$  and  $\mathbf{P}_k^{n+1}$  when  $i \neq k$ . Therefore, the system can be solved without root searching iterations as follows. We first solve the linear equation (29) for  $\mathbf{P}_i^{n+1}$  for every index  $i$  separately, which amounts to inverting a  $3 \times 3$  matrix for every  $i$ . Then  $\mathbf{X}_i^{n+1}$  and  $\mathbf{Y}_J^{n+1}$  are advanced explicitly according to Eqs. (27) and (30), and the last step is to advance  $\mathbf{A}_J^{n+1}$ , also explicitly, according to Eq. (28).

The preservation of the symplectic structure exerts  $D(2D-1)$  constraints on the numerical solution. Because  $D$  is a large number, preservation of symplectic structure is a very strong constraint and significantly reduces the errors of numerical solutions. We can also appreciate this advantage from the viewpoint of symplectic capacity, which is defined on any open set of the phase space. Symplectic maps preserve symplectic capacity [34], and in principle there are infinite constraints that symplectic algorithms can satisfy as the continuous systems do.

We now apply this canonical symplectic PIC scheme to simulate the nonlinear Landau damping process. This study also serves as a test of the algorithm. Previously, similar study and test have been performed for other algorithms, e.g., the Eulerian algorithms for the Vlasov-Poisson system [22, 35]. The ions are treated as a uniform positively charged background, and the dynamics of electrons are simulated. The electron density is  $n_e = 1.149 \times 10^{16}/m^3$ , and the thermal velocity of electrons is  $v_T = 0.1c$ , where  $c$  is the light velocity in vacuum. The three-dimensional computational region is divided into  $896 \times 1 \times 1$  cubic cells. The size of grid is chosen to be  $\Delta x = 2.4355 \times 10^{-4}m$ , the time step  $\Delta t = \Delta x/2c$ .

The interpolation function is chosen to be 8th order, i.e.,

$$W(\mathbf{x}) = W_1(x/\Delta x)W_1(y/\Delta x)W_1(z/\Delta x), \quad (31)$$

$$W_1(q) = \begin{cases} 0, & q > 2, \\ \frac{15}{1024}q^8 - \frac{15}{128}q^7 + \frac{49}{128}q^6 - \frac{21}{32}q^5 + \frac{35}{64}q^4 - q + 1, & 1 < q \leq 2, \\ -\frac{15}{1024}q^8 - \frac{15}{128}q^7 + \frac{7}{16}q^6 - \frac{21}{32}q^5 + \frac{175}{256}q^4 - \frac{105}{128}q^2 + \frac{337}{512}, & 0 < q \leq 1, \\ -\frac{15}{1024}q^8 + \frac{15}{128}q^7 + \frac{7}{16}q^6 + \frac{21}{32}q^5 + \frac{175}{256}q^4 - \frac{105}{128}q^2 + \frac{337}{512}, & -1 < q \leq 0, \\ \frac{15}{1024}q^8 + \frac{15}{128}q^7 + \frac{49}{128}q^6 + \frac{21}{32}q^5 + \frac{35}{64}q^4 + q + 1, & -2 < q \leq -1, \\ 0, & q < -2. \end{cases} \quad (32)$$

It can be proved that the kernel function  $W$  is 3rd order continuous in the whole space. According to our performance benchmarks, this 8th order kernel is about 30% more computationally costly than a 2nd order kernel, which is acceptable since a higher order continuous kernel gives more numerical fidelity. Initially,  $10^5$  sampling points of electrons are distributed in each cell. The total number of particles is  $N = 8.96 \times 10^7$ , and the number of degrees of freedom is  $D = 2.69 \times 10^8$ . The initial electrical field perturbation is  $\mathbf{E}_1 = E_1 \cos(kx) \mathbf{e}_x$ , where the wave number is  $k = 2\pi/224\Delta x$ , and the amplitude of the perturbation electric field is  $E_1 = 9.103 \times 10^4 V/m$ . The simulations are performed for 80000 time steps, during which a complete picture of the nonlinear Landau damping is revealed. As expected for symplectic algorithms, the numerical error of energy does not increase with time and is bounded within 1% for all time. The theoretical damping rate calculated from the dispersion relation is  $\omega_i = -1.3926 \times 10^9/s$ , and the theoretical real frequency is  $\omega_r = 9.116 \times 10^9/s$ . In Fig. 1, the slope of the green line is the theoretical damping rate, and the blue curve is the evolution of the electrical field observed in the simulation. It is evident that the simulation and theory agree perfectly. After  $t = 30/\omega_r$ , the energy of the wave drops below the level of numerical noise, and the damping process stops. The evolution of the electron distribution function is plotted in Fig. 2, which clearly demonstrates the mechanism of phase mixing in velocity space. We observe in Fig. 2 that the wave-number in velocity space increases with time, which results in a decrease in density perturbation and thus attenuation of the electrical field. More importantly, this mechanism of phase mixing is the dominant physics for the entire nonlinear evolution of the Landau damping, as proved by Mouhot and Villani [27, 28] recently for the electrostatic Vlasov-Poisson system. In addition, our simulation is electromagnetic and it shows that this physical picture of nonlinear Landau damping is also valid for the electromagnetic Vlasov-Maxwell system, as Villani conjectured [29]. It is the

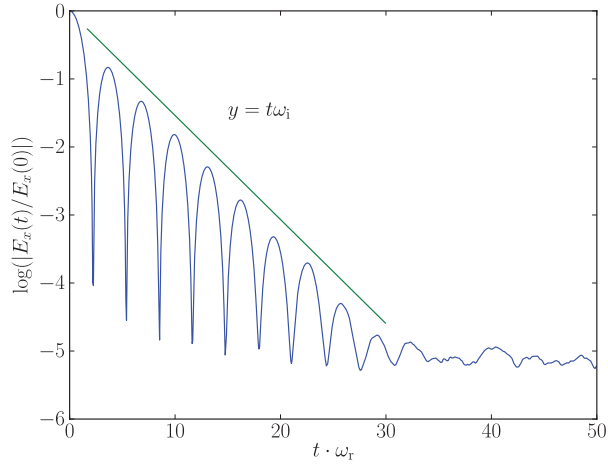


FIG. 1. Perturbed electrical field as a function of time. The slope of the green line is the theoretical damping rate.

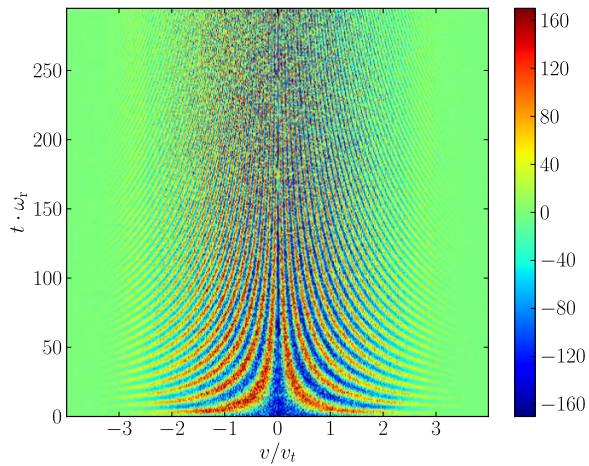


FIG. 2. Electron distribution function in velocity space as a function of time. Different colors denote the amplitude of the perturbation. The mechanism of phase mixing in velocity space is clearly demonstrated. The wave-number in velocity space increases with time, which results in a decrease in density perturbation and thus attenuation of the electrical field.

long-term accuracy and fidelity of the canonical symplectic PIC algorithm that enables the confirmation of Mouhot and Villani's theory and conjecture over several orders of magnitude.

Even though Mouhot and Villani rigorously proved that when the initial perturbation amplitude is small enough, the electrical perturbation will decay to zero, plasma physicists

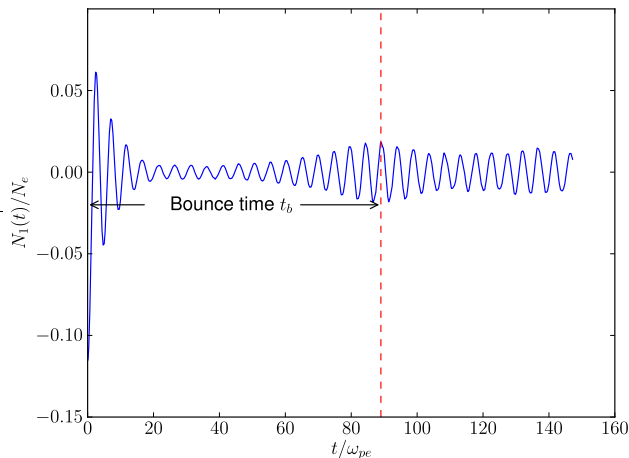


FIG. 3. In nonlinear Landau damping, the perturbation will bounce back after initial phase of damping if the initial perturbation is large enough. The amplitude of the initial electric field in this case is 0.494MV/m.

have known this fact since 1960s [36, 37]. It has also been known that when the initial electrical perturbation is large enough, the perturbation will bounce back after initial phase of damping [36, 37]. One such case simulated is plotted in Fig. 3. For this case, the amplitude of the initial electrical field is 0.494MV/m and the wave number is  $k = 2\pi/272\Delta x$ . Figure 4 shows the bounce-time as a function of the initial amplitude of the electrical field obtained in simulations. The physics demonstrated in our PIC simulations agrees with that obtained from Eulerian solvers [35], except that our simulations are carried out for the full Vlasov-Maxwell system.

In the second application, the 1D nonlinear mode conversion of extraordinary waves to electron Bernstein waves (X-B mode conversion) in a inhomogeneous hot plasma is simulated for a long time. The plasma density profile in the simulation is

$$n_e(x) = n_0 \begin{cases} \exp \left[ - \left( \frac{x/\Delta x - n_r - 320}{0.4n_r} \right)^2 \right], & 0 < \frac{x}{\Delta x} \leq (n_r + 320), \\ 1, & (n_r + 320) < \frac{x}{\Delta x} \leq 1300, \end{cases} \quad (33)$$

where  $n_0 = 2.3 \times 10^{19} \text{ m}^{-3}$ ,  $n_r = 380$ , and  $\Delta x = 2.773 \times 10^{-5} \text{ m}$  is the grid size. The thickness of the plasma boundary is  $n_r \Delta x$ . The electron temperature is  $T_e = 57.6 \text{ eV}$ , and constant external magnetic field is  $\mathbf{B} = B_0 \mathbf{e}_z$  with  $B_0 = 0.6 \text{ T}$ . The simulation domain is a  $1584 \times 1 \times 1$  cubic mesh. At both boundaries in the  $x$ -direction, the Mur's absorbing

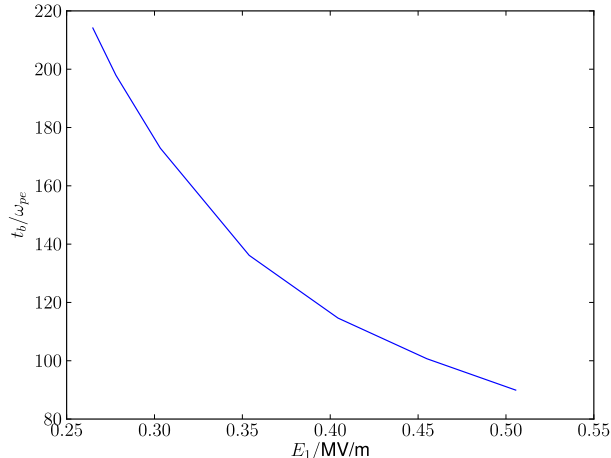


FIG. 4. Relationship between the initial amplitude  $E_1$  and the bounce time  $t_b$  in nonlinear Landau damping.

condition are used, and periodic boundary conditions are adopted in the  $y$ - and  $z$ -directions. The time step is chosen to be  $\Delta t = \Delta x/2c$ . At the left boundary, a source is placed to excite an electromagnetic perturbation at  $\omega = 0.0145/\Delta t$  with  $\mathbf{E}_1 = E_1 \mathbf{e}_y$  and  $E_1 = 900\text{kV}$ . As illustrated in Fig. 5, the extraordinary wave excited at the left boundary first propagates to the region of cutoff-resonance-cutoff near  $x/\Delta x = 500$ . The wave is then partially reflected back, and partially converted to electron Bernstein waves [24]. The reflectivity evolution is plotted in Fig. 6. Nonlinear excitations and self-interactions of the Bernstein modes dominate the long time dynamics of the mode conversion process. As a consequence, the reflectivity of the incident wave evolves nonlinearly as shown in Fig. 6. For this set of chosen parameters, the incident wave is completely reflected at the later time of the process.

In conclusion, we have developed a canonical symplectic particle-in-cell simulation method for the Vlasov-Maxwell system by discretizing its canonical Poisson bracket. In phase space, the distribution function is discretized by the Klimontovich representation using Lagrangian markers, and the electromagnetic field is discretized point-wise on a spatial grid. The resulting canonical Hamiltonian system with a large number of degrees of freedom is integrated by the symplectic Euler method, whose difference equations can be solved inexpensively by inverting a  $3 \times 3$  matrix locally for every particle. Implicit root searching and global matrix inversion are avoided entirely. This technique makes large-scale applications of the developed canonical symplectic PIC method possible. To suppress numerical

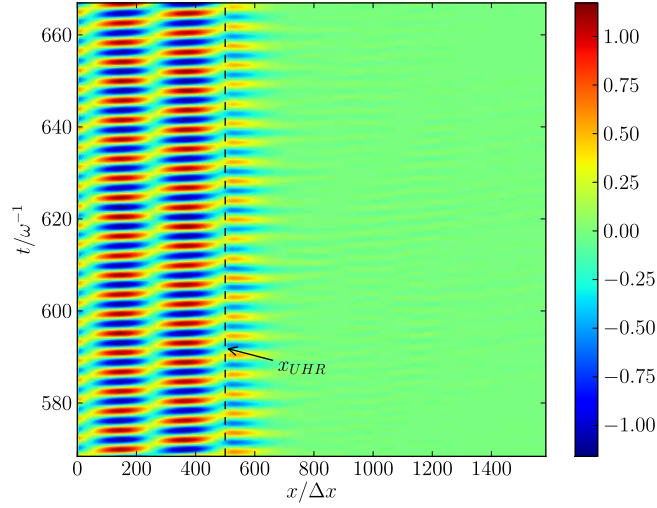


FIG. 5. The space-time dependence of  $E_y(t, x)$  during the nonlinear X-B mode conversion.

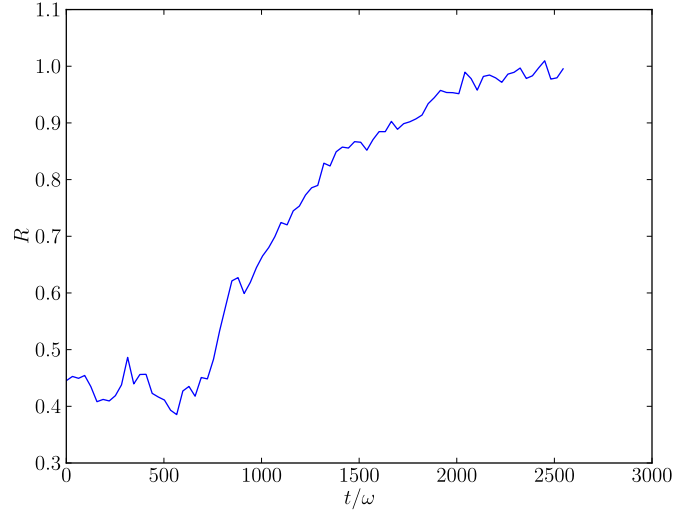


FIG. 6. The evolution of reflectivity during the nonlinear X-B mode conversion.

noise caused by the coarse sampling, smoothing functions for sampling points can also be conveniently implemented in the canonical symplectic PIC algorithm. By incorporating the smoothing functions into the Hamiltonian functional before the discretization, we are able to rein in all the benefits of smoothing functions without destroying the canonical symplectic structure. Progress in this and other directions will be reported in future publications.

## ACKNOWLEDGMENTS

This research is supported by ITER-China Program (2015GB111003, 2014GB124005, 2013GB111000), JSPS-NRF-NSFC A3 Foresight Program in the field of Plasma Physics (NSFC-11261140328), the CAS Program for Interdisciplinary Collaboration Team, the Geo-Algorithmic Plasma Simulator (GAPS) project, and the the U.S. Department of Energy (DE-AC02-09CH11466).

- 
- [1] C. K. Birdsall and A. B. Langdon. *Plasma Physics via Computer Simulation*. Adam Hilger, Bristol.
  - [2] R. W. Hockney and J. W. Eastwood. *Computer Simulation Using Particles*. Institute of Physics Publishing, Bristol, 1988.
  - [3] J. Boris. In *Proceedings of the Fourth Conference on Numerical Simulation of Plasmas*, page 3. Naval Research Laboratory, Washington D. C., 1970.
  - [4] J. P. Boris. Dynamic stabilization of the imploding shell rayleigh-taylor instability. *Comments Plasma Phys. Controlled Fusion*, 3:1, 1977.
  - [5] J. Villasenor and O. Buneman. Rigorous charge conservation for local electromagnetic field solvers. *Computer Physics Communications*, 69:306, 1992.
  - [6] R. D. Ruth. A canonical integration technique. *IEEE Trans. Nucl. Sci*, 30:2669, 1983.
  - [7] K. Feng. On difference schemes and symplectic geometry. In K. Feng, editor, *the Proceedings of 1984 Beijing Symposium on Differential Geometry and Differential Equations*, pages 42–58. Science Press, 1985.
  - [8] K. Feng. Difference schemes for Hamiltonian formalism and symplectic geometry. *J. Comput. Maths.*, 4:279–289, 1986.
  - [9] Kang Feng and Mengzhao Qin. *Symplectic Geometric Algorithms for Hamiltonian Systems*. Springer-Verlag, 2010.
  - [10] E. Forest and R. D. Ruth. 4th-order symplectic integration. *Physica D*, 43:105–117, 1990.
  - [11] P. J. Channell and C. Scovel. Symplectic integration of Hamiltonian systems. *Nonlinearity*, 3:231–259, 1990.
  - [12] J. Candy and W. Rozmus. A symplectic integration algorithm for separable Hamiltonian

- functions. *Journal of Computational Physics*, 92:230–256, 1991.
- [13] J. E. Marsden and M. West. Discrete mechanics and variational integrators. *Acta Numerica*, 10:357–514, 2001.
- [14] E. Hairer, C. Lubich, and G. Wanner. *Geometric Numerical Integration: Structure-Preserving Algorithms for Ordinary Differential Equations*. Springer, New York, 2002.
- [15] H. Qin and X. Guan. A variational symplectic integrator for the guiding center motion of charged particles for long time simulations in general magnetic fields. *Physical Review Letters*, 100:035006, 2008.
- [16] H. Qin, X. Guan, and W. M. Tang. Variational symplectic algorithm for guiding center dynamics and its application in tokamak geometry. *Physics of Plasmas*, 16:042510, 2009.
- [17] H. Qin, S. Zhang, J. Xiao, J. Liu, Y. Sun, and W. M. Tang. Why is boris algorithm so good? *Physics of Plasmas*, 20:084503, 2013.
- [18] R. Zhang, J. Liu, H. Qin, Y. Wang, Y. He, and Y. Sun. Volume-preserving algorithm for secular relativistic dynamics of charged particles. *Physics of Plasmas*, 22:044501, 2015.
- [19] Y. He, Y. Sun, J. Liu, and H. Qin. Volume-preserving algorithms for charged particle dynamics. *Journal of Computational Physics*, 281:135, 2015.
- [20] J. Squire, H. Qin, and W. M. Tang. Geometric integration of the Vlasov-Maxwell system with a variational particle-in-cell scheme. *Physics of Plasmas*, 19:084501, 2012.
- [21] J. Y. Xiao, J. Liu, H. Qin, and Z. Yu. A variational multi-symplectic particle-in-cell algorithm with smoothing functions for the Vlasov-Maxwell system. *Physics of Plasmas*, 20:102517, 2013.
- [22] M. Kraus. *Variational integrators in plasma physics*. PhD thesis, Technical University of Munich, 2014.
- [23] B. A. Shadwick, A. B. Stamm, and E. G. Evstatiev. Variational formulation of macro-particle plasma simulation algorithms. *Physics of Plasmas*, 21:055708, 2014.
- [24] J. Xiao, J. Liu, H. Qin, Z. Yu, and N. Xiang. Variational symplectic particle-in-cell simulation of nonlinear mode conversion from extraordinary waves to Bernstein waves. *Physics of Plasmas*, page in press, 2015.
- [25] E. Evstatiev and B. Shadwick. Variational formulation of particle algorithms for kinetic plasma simulations. *J. Comput. Phys.*, 245:376, 2013.
- [26] J. E. Marsden and A. Weinstein. The Hamiltonian structure of the Maxwell-Vlasov equations.

- Physica*, 4D:394, 1982.
- [27] C. Mouhot and C. Villani. On Landau damping. *Acta Mathematica*, 207:29, 2011.
- [28] C. Villani. Particle systems and nonlinear Landau damping. *Physics of Plasmas*, 21:030901, 2014.
- [29] C. Villani. Plasmataalks: Ron Davidson interviews Cedric Villani, 2014.
- [30] P. J. Morrison. The Maxwell-Vlasov equations as a continuous Hamiltonian system. *Physics Letters*, 80A:383, 1980.
- [31] A. Weinstein and P. J. Morrison. Comments on: The Maxwell-Vlasov equations as a continuous Hamiltonian system. *Physics Letters*, 86A:235, 1981.
- [32] P. J. Morrison. Hamiltonian field description of two dimensional vortex fluids and guiding center plasmas. Technical Report PPPL-1783, Princeton Plasma Physics Laboratory, 1981.
- [33] P. J. Morrison. Hamiltonian field description of the one-dimensional Poisson-Vlasov equations. Technical Report PPPL-1788, Princeton Plasma Physics Laboratory, 1981.
- [34] H. Hofer and E. Zehnder. *Symplectic invariants and Hamiltonian dynamics*. Birkhauser Verlag, 1994.
- [35] T. Zhou, Y. Guo, and C. W. Shu. Numerical study on Landau damping. *Physica D*, 157:322, 2001.
- [36] T. P. Armstrong. Numerical studies of the nonlinear Vlasov equation. *Physics of Fluids*, 6:1269, 1967.
- [37] J. Canosa and J. Gazdag. Threshold conditions for electron trapping by nonlinear waves. *Physics of Fluids*, 17:2030, 1974.